Rheologica Acta Rheol Acta 26: 499–507 (1987)

A pseudo-time integral method for non-isothermal viscoelastic flows and its application to extrusion simulation

X.-L. Luo and R. I. Tanner

Department of Mechanical Engineering, University of Sydney, Sydney (Australia)

Abstract: A pseudo-time integral scheme based on a finite streamline element method is developed to combine variable temperature with viscoelasticity. A specific KBKZ integral model for isothermal flow is transformed to its non-isothermal version by introducing a pseudo-time and applying the Morland-Lee hypothesis. The coupling between momentum and energy equations is through the time-temperature shifting factor by which the pseudo-time is defined. The observer time and the pseudo-time are simultaneously calculated when tracing the strain history for the stress calculation in a non-homogeneous temperature field. Using this scheme, a full non-isothermal numerical simulation of some IUPAC extrusion experiments is carried out. Results show that while the temperature distribution near the die exit plane is an important factor controlling extrudate swell, either self-heating inside the die tube or external cooling on the free surface dominantly determines the temperature distribution near the die exit when the wall temperature is kept constant, depending on whether the Péclet number is large or small. The hot layer effect predicted by the inelastic swell mechanism is confirmed and well illustrated by the computation. Calculations with reasonable thermal boundary conditions further convince us that the isothermal assumption in our earlier numerical simulation is a good approximation in this particular case.

Key words: Time-temperature superposition, extrusion swell, Péclet number

1. Introduction

It is well known that the effects of temperature change are often very important in many polymer processing processes [1]. Thermally-induced extrudate swell and the film blowing process are two well-illustrated examples. Phuoc and Tanner [2] investigated the swelling of Newtonian extrudates where the viscosity varies with $e^{-\alpha \Delta T}$. Energy dissipation created a hot fluid near the centreline while the die wall was maintained at constant temperature. Ambient temperature was lower than wall temperature and caused a heat loss from the extrudate. The swelling was remarkably high ($\sim$ 70%) compared with the isothermal case and a good correlation with the results of the inelastic swelling mechanism [3] was obtained. This result was latter qualitatively confirmed by other work [4]. In a numerical simulation of film blowing experiments, Luo and Tanner found [5] that the inclusion of temperature modelling was a great improvement over the isothermal case. The isothermal calculation resulted in bubbles not close to observed shapes, while by defining a proper heat transfer coefficient to take care of heat losses by convection and radiation from both sides of the film the bubble shapes as well as the temperature profiles obtained were very close to experimentally observed ones.

In Newtonian cases, the coupling between momentum and energy equations is directly through temperature-induced variations of viscosity, while in non-Newtonian cases the matter is in general more complicated and the time-temperature shifting concept is often very useful. Suppose the rate of a rheological process of a material is determined by an internal time-scale (or clock) within the material. As temperature rises, so does the amount of molecular motion occuring in one unit of an observer's time; the material's internal time scale shortens so that the process proceeds faster.

Let us consider a material undergoing stress relaxation. Suppose the material time-scale changes so that one unit of material time is now equivalent to $a(T)$ units of observer time; $a(T)$ is a decreasing function of temperature T. Let $G(t, T)$ be the stress relaxation modulus at temperature T, and let $G(t) = G(t, T_0)$ be the stress relaxation modulus at a reference temperature T_0. Applying the time-temperature shifting concept, we have

$$G(t, T) = \left(\frac{\varrho T}{\varrho_0 T_0}\right) G\left(\frac{t}{a(T)}\right) \tag{1}$$

where the factor $(\varrho T/\varrho_0 T_0)$ is usually nearly unity and can often be ignored in practice. In addition to the relaxation modulus, other characteristic linear viscoelastic quantities can be dealt with in the same manner. Although time-temperature shifting enables one to determine fluid properties at a temperature T given a master curve at T_0 one still has to consider situations in which a particle in a flow will encounter a continuous temperature variation. Morland and Lee [6] showed how to incorporate time-temperature shifting into linear viscoelastic boundary-value problems. In this case a pseudo-time ξ can be introduced where ξ is the time measured by the particle's own internal "clock". The amount of time that elapses during an interval $d\xi$ of pseudo-time is given by $dt/a(T)$ where $a(T)$ is the time-shifting fator. Then we define

$$\xi = \int_0^t a^{-1}(T(t'))\, dt' \tag{2}$$

and reformulate the problem in terms of ξ.

The Morland-Lee hypothesis can clearly be applied to the non-linear single integral models, which is the main goal of the present paper. In the next section we will describe in detail the pseudo-time integral scheme for non-isothermal problems. It will be seen that the time-temperature shifting is in principle a straightforward way of obtaining the non-isothermal form for the particular KBKZ integral model and our streamline element integral scheme [4, 7, 10], initially developed for isothermal problems, can be modified to combine variable temperature with viscoelasticity without major program changes if we work with both the observer time and the pseudo-time when integrating the non-isothermal stresses. In Section 3 a full non-isothermal simulation of some IUPAC extrusion experiments, for which a thorough isothermal simulation has already been done [7, 10], is carried out. Some interesting aspects such as the proper thermal boundary conditions, the factor of self-heating, the rule played by the Péclet number and the hot layer effect are discussed in the process. Our conclusions are given in the last section.

2. Pseudo-time integral scheme

Before describing our time-temperature shifting technique, we need to sketch the main iterative features of the present program [4, 7]. For a particular non-isothermal viscoelastic flow problem, we first solve the corresponding Newtonian creeping flow problem, starting with a proper initial temperature field. With the known velocity and temperature fields, the differential or the integral constitutive equations are solved for the non-Newtonian stresses by integrating along streamlines. These non-Newtonian stresses are then applied as pseudo-body forces to the next iteration for new velocity and temperature fields and this process is repeated until both velocity and temperature fields converge. This non-isothermal iteration scheme was first tested by solving the thermally-induced extrudate swell problem for Newtonian fluid with exactly the same kinematic and thermal boundary conditions as those used by Phuoc and Tanner [2]. The two results turned out to agree very well [4]. We also did the problem of viscous heating in capillary flow for a power-law fluid with viscosity-temperature dependence, in which information on both velocity gradients and temperature obtained from the previous iteration has to be used to calculate the power-law stress for the new iteration:

$$\boldsymbol{\tau}_m = \varkappa\, e^{-\alpha T_{m-1}} \left(\sqrt{2\,\mathrm{tr}\,(\boldsymbol{e}^2)}\right)^{n-1} \boldsymbol{e}_{m-1} \tag{3}$$

where m and $m-1$ denote the iteration indexes and $\boldsymbol{e}$ is the rate-of-strain tensor. For Newtonian liquids, Kearsley [8] obtained an exact solution to this problem. To further check the accuracy of our non-Newtonian and non-isothermal iteration scheme, we let the power-law index n equal 1.0 and treat the Newtonian stress as a pseudo-body force, i.e., as a real non-Newtonian problem. Eq. (3) was actually used and every part of the entire streamline element scheme for non-isothermal and non-Newtonian problems was tested. With 5×15 elements and four iterations our finite element results showed relative errors of less than 5×10^{-5} and 7×10^{-5} in temperature and axial velocity fields respectively.

For the differential type ot constitutive equations, including the generalized Newtonian models, once we have the correct non-isothermal version of the model, the non-isothermal stress calculation imposes little extra difficulty, for only instantaneous temperature values are required locally and are readily provided in a similar manner to the velocity gradients. The non-

isothermal stress calculation for an integral model in general turned out to be more complicated. Consider a special form of the integral model

$$\tau_{ij}(t) = \int_{-\infty}^{t} M(t-t')\, H_{ij}(t')\, dt' \tag{4}$$

where $M(t-t')$ is the time dependent memory function and $H_{ij}(t')$ is the kernel function depending on strain tensors and their invariants. From (4) we have, in an isothermal case, that the contribution to the stress at time t is $M(t-t')\, H_{ij}(t')\, dt'$ due to strain at t' and in the interval dt'. In the non-isothermal case, the stress contribution is, using the Morland-Lee hypothesis and ignoring the near-unity factor $(\varrho T/\varrho_0 T_0)$,

$$d\tau_{ij} = M(\xi - \xi')\, H_{ij}(t')\, d\xi' \tag{5}$$

where ξ is the pseudo-time defined by eq. (2). Hence the total stress at time t is

$$\tau_{ij} = \int_{-\infty}^{\xi(t)} M(\xi - \xi')\, H_{ij}(t')\, d\xi'. \tag{6}$$

Note in (5) and (6) $d\xi'$ instead of dt' should be used and the upper limit should be changed from t to $\xi(t)$ accordingly; this can easily be checked by calculating the simple shear stress of the Maxwell integral model with a constant time-temperature shifting factor. Eq. (6) simply tells us that in terms of the pseudo-time, viscoelastic laws for a nonhomogeneous temperature field take the same form as for a uniform temperature field. The specific isothermal form of eq. (4) we have been working on is that proposed by Papanastasiou *et al.* [9, 7],

$$\boldsymbol{\tau}(t) = \int_{-\infty}^{t} \left[\sum \frac{a_k}{\lambda_k} \exp\left(-\frac{t-t'}{\lambda_k} \right) \right] \cdot \frac{\alpha}{(\alpha - 3) + \beta I_{c^{-1}} + (1-\beta)\, II_{c^{-1}}} \boldsymbol{C}_t^{-1}(t')\, dt' \tag{7}$$

where λ_k and a_k are the relaxation times and relaxation modulus coefficients at a reference temperature T_0 respectively, and $\boldsymbol{C}_t^{-1}(t')$ is the Finger strain tensor. This model form was latter modified by us [10] to take into account the second normal stress and to improve its elongational predictions for low-density polyethylene melts. For simplicity, we will use the original form to describe our pseudo-time integral scheme; the formulation for the modified form follows the same pattern. The non-isothermal version of (7), following eq. (6), can then be written as

$$\boldsymbol{\tau}(t) = \int_{-\infty}^{\xi(t)} \left[\sum \frac{a_k}{\lambda_k} \exp\left(-\frac{\xi - \xi'}{\lambda_k} \right) \right] \cdot \frac{\alpha}{(\alpha - 3) + \beta I_{c^{-1}} + (1-\beta)\, II_{c^{-1}}} \boldsymbol{C}_{t(\xi)}^{-1}(t'(\xi'))\, d\xi'. \tag{8}$$

To see that the $a(T)$ appearing in the definition of pseudo-time is a time-shift factor we may calculate the mean relaxation time of model eq. (8) with a constant value of $a(T)$,

$$\lambda(T) = \frac{\int_{-\infty}^{t} \sum a_k e^{-\frac{\xi - \xi'}{\lambda_k}} (t-t')\, dt'}{\int_{-\infty}^{t} \sum a_k e^{-\frac{\xi - \xi'}{\lambda_k}} dt'}.$$

Here the integral variable is t' since the mean relaxation time is defined in terms of observer time. Now from (2) $t - t' = a(T)(\xi - \xi')$ and $dt' = a(T)\, d\xi'$, using this variable transformation the above equation becomes,

$$\lambda(T) = \frac{a^2(T)}{a(T)} \left[\frac{\int_{-\infty}^{\xi} \sum a_k e^{-\frac{\xi - \xi'}{\lambda_k}} (\xi - \xi')\, d\xi'}{\int_{-\infty}^{\xi} \sum a_k e^{-\frac{\xi - \xi'}{\lambda_k}} d\xi'} \right],$$

the expression in the square parenthesis is immediately recognised as the mean relaxation time at reference temperature T_0. So we have $\lambda(T) = a(T)\, \lambda(T_0)$.

It should be noted that the viscoelastic law (8) is on the whole expressed in (x, ξ) coordinates, while the expression for strain tensors in (8) as well as the usual conservation laws are expressed in (x, t) coordinates. It is this mixed feature that causes extra difficulties in non-isothermal stress calculations for integral models of the present type.

One alternative way to calculate (8) is to work with the observer time t' by taking definition (2) as the suitable integral variable transformetion. Thus $d\xi'$ becomes $a(T)\, dt'$ and the isothermal strain kernel function is recovered. Unfortunately the expression $\exp\left(-\frac{\xi(t) - \xi'(t')}{\lambda_k} \right)$ becomes so complicated in terms of t and t' that it inhibits the use of the existing efficient Laguerre integration scheme [7] in our program, and so we decided not to take that alternative. The advantage of working with pseudo-time ξ' is that the exponential part of the integral function takes exactly the same form as in the isothermal case and the existing Laguerre integration scheme for the isothermal case can be directly employed. However it should also be kept in mind that in our existing streamline element scheme [7] the calculation of the Cauchy strain tensor is through the relations $\boldsymbol{C}_t(t') = \boldsymbol{F}_t^T(t')\, \boldsymbol{F}_t(t')$ and $d\boldsymbol{F}_t(t')/dt' = \boldsymbol{L}(t')\, \boldsymbol{F}_t(t')$ which are completely expressed in (x, t) coordinates. Now the key matter is to calculate $\boldsymbol{C}_{t(\xi)}^{-1}(t'(\xi'))$ at the right points required by the Laguerre rule in terms of pseudo-time. Because the

solution of the velocity and temperature fields are provided in terms of streamline element coordinates which are directly connected with (x, t) coordinates, the most convenient way to calculate strain tensors in non-isothermal cases is still to work with the observer time t' as in isothermal cases. Considering the k-th relaxation time, the Laguerre points for it are given by

$$\xi - \xi_k'^m = \lambda_k s_n^m \tag{9}$$

where s_n^m is the m-th abscissa for the n-point Laguerre quadrature. The corresponding value of observer time is then, from (2),

$$t(\xi) - t'(\xi') = \int_0^{\lambda_k s_n^m} a[T(t''(\xi''))]\, d\xi''. \tag{10}$$

Unfortunately, $T(t''(\xi''))$ is unknown to us since solution of the temperature field is in terms of observer time t'' and before calculation of (10) we do not know the function $t''(\xi'')$. Now we see from a computational point of view that the inverse function of pseudo-time cannot be evaluated by a simple integration. To avoid calculating the inverse function of pseudo-time, we found the differential form of eq. (2) was more useful,

$$d\xi = a^{-1}(T(t'))\, dt'. \tag{11}$$

Let Δl_i be the length of a typical streamline segment described in [7], V_i and T_i be the magnitudes of average velocity and temperature along the streamline segment. The residence time or observer time of the particle can then be approximated by

$$\Delta t_i' = \frac{\Delta l_i}{V_i}. \tag{12}$$

From (11) the pseudo-time is readily evaluated as

$$\Delta \xi' = \frac{\Delta l_i}{V_i\, a(T_i)} \tag{13}$$

where the values of Δl_i, V_i and T_i can easily be calculated by using the natural element interpolation functions. As described in [7], the observer time $t - t'$ is calculated backwards through a piecewise summation. Obviously the same procedure applies equally to the pseudo-time, i.e., during the strain history tracing process, we simultaneously calculate the two time systems and keep recording both of them. In this way we have numerically established a one-to-one correspondence between observer time and pseudo-time. With this one-to-one correspondence, the rest of the task is simple and most of the routines for strain tensor calculation in the isothermal case are directly employed with little change: the pseudo-time points $\xi_k'^{(m)}$ defined by (9) are located in exactly the same way as the observer time points for the isothermal case, then we can find the corresponding observer time through the one-to-one correspondence between the two parallel time systems. With the locations of Laguerre points known in terms of observer time, the strain tensor calculation is exactly the same as described in [7]. Finally, the same Laguerre integration scheme is employed to calculate the non-isothermal stresses.

3. Non-isothermal modelling of extrusion experiments

Non-isothermal extrusion calculations for Newtonian and power-law fluids have been done by Phuoc and Tanner [2, 11]. It was found that under the thermal boundary conditions being used, increasing the Nahme-Griffith number Na causes an increase in swelling and so does increasing the power-law index. The temperature distribution near the exit plane was found to be a critical factor determining whether the extrudate would swell or contract relative to the isothermal case. Here we shall attempt a full non-isothermal and non-Newtonian extrusion calculation using the KBKZ integral model and the pseudo-time stress integral scheme described in the previous section. The extrusion experiments to be modelled were carried out by one of the IUPAC groups and the results were reported by Meissner [12]. Our isothermal simulation of these experiments were presented in [7] and [10].

3.1 Nondimensionalization and thermal boundary conditions

For simplicity, only the energy equation is discussed here,

$$\varrho C V_i \frac{\partial T}{\partial X_i} - \varkappa \frac{\partial^2 T}{\partial X_j^2} - \sigma_{ij} e_{ij} = 0 \tag{14}$$

with possible convection boundary conditions on some surface S_q,

$$\varkappa \frac{\partial T}{\partial n} = -h(T - T_\infty) \tag{15}$$

where ϱ, C, $\varkappa$ are the fluid density, thermal capacity and thermal conductivity respectively, h is the local heat transfer coefficient and T_∞ is the surrounding temperature. The constitutive equation is modified from (8) with β replaced by β_k and the $C_t(t')$ term added [10]. In this case each relaxation mode has its own value of $\beta(\beta_k)$, and $C_t^{-1}(t')$ is replaced by $(1-\theta)^{-1}\{C_t^{-1}(t') + \theta C_t(t')\}$; where θ is a constant $(0 \leqq \theta < 1)$. These modifications permit much better modelling of the elongational behaviour and the sec-

ond normal-stress difference [10]. Define the basic non-dimensionalised variables as

$$x_j^* = \frac{x_j}{R}, \quad T^* = \frac{T - T_0}{T_0 - T_\infty}, \quad V_j^* = \frac{V_j}{\bar{W}}, \quad \sigma^* = \frac{\sigma R}{\eta_0 \bar{W}},$$

where R is the die radius, η_0 is the zero-shear-rate viscosity of the model at reference temperature T_0, $\eta_0 = \sum a_k \lambda_k$, and $\bar{W}$ is a characteristic velocity in the flow which will be defined later. With these basic non-dimensionalised variables (14) and (15) can be re-written as

$$Pe\, V_j^* \frac{\partial T^*}{\partial x_i^*} - \frac{\partial^2 T^*}{\partial x_i^{*2}} - Br\, \sigma_{ij}^* e_{ij}^* = 0, \tag{16}$$

$$\frac{\partial T^*}{\partial n^*} = -Nu\,(T^* + 1) \tag{17}$$

where

$$Pe = \frac{\varrho C R \bar{W}}{\varkappa}$$

is the Péclet number indicating the ratio of heat convection to conduction,

$$Br = \frac{\eta_0 \bar{W}^2}{\varkappa (T_0 - T_\infty)}$$

is the Brinkmann number indicating the importance of self-heating versus external heating, and

$$Nu = R \frac{h}{\varkappa}$$

is the Nusselt number. A number closely related to the Péclet number is the Graetz number $Gz = Pe\,(R/L)$ which can be understood to be the ratio of the time required for heat conduction from the centre of the die tube to the wall and the average residence time of particles in the die tube. This number is usually larger than the die length/radius ratio in extrusion process which means the fully developed temperature is rarely achieved. The coupling between the momentum and the energy equations is through the time-temperature shifting factor $a\,(T)$ which appears in the definition of pseudo-time ξ. For low-density polyethylene (LDPE) the following form for $a\,(T)$ is adequate [1],

$$a\,(T) = \frac{\eta}{\eta_0} = \exp\left[-\frac{E_0}{R_0}\left(\frac{1}{T} - \frac{1}{T_0}\right)\right], \tag{18}$$

where E_0 is the activation constant and R_0 the gas constant. The temperature coefficient of the material at reference temperature T_0 can be determined from (18) by expanding $E_0/R_0\,T$ around T_0,

$$a\,(T_0) = \frac{E_0}{R_0 T_0^2}.$$

Thus the Nahme-Griffith number is given by

$$Na = \frac{\bar{W}^2 \eta_0 \alpha\,(T_0)}{\varkappa R} = \frac{\bar{W}^2 \eta_0 E_0}{\varkappa R R_0 T_0^2}. \tag{19}$$

A large Nahme-Griffith number indicates a strong coupling between momentum and energy equations. Regarding the thermal extrusion problem, five dimensionless groups can be formed so that the swelling ratio is a function of them all,

$$\chi = \chi\,(Wi, Pe, Nu, Br, Na) \tag{20}$$

where Wi is the Weissenberg number. A thorough investigation into the numerous combined effects of all five dimensionless groups under different boundary conditions is no doubt a tremendous task and it was found [11] that a simple linear superposition of two separated non-Newtonian and non-isothermal results does not in general give the combined effects. However, it is feasible and of practical interest to numerically estimate the thermal effects of some well-defined actual extrusion experiments, especially when a successful isothermal but non-Newtonian modelling has already been carried out [7, 10]. The isothermal modelling of the IUPAC extrusion experiments [12] gave results in close agreement with experiment data except at high apparent shear rate $\bar{D} \equiv Q/4R^3 = 10\ \mathrm{s}^{-1}$. Our isothermal calculation much overpredicted the swelling ratio at $\bar{D} = 10\ \mathrm{s}^{-1}$. One possible explanation to this disagreement would be a "hot layer" effect: although the wall temperature in the experiment was kept at constant value $T_w = 150\,°$, the self-heating at the die wall might become significant at $\bar{D} = 10\ \mathrm{s}^{-1}$ and a hot layer may form near the die exit. This hot layer, according to the inelastic swelling mechanism [3], would cause the extrudate to swell less than under true isothermal conditions. To qualitatively investigate this possibility a full non-isothermal modelling is needed and this in fact was the initial motivation of this numerical work. Thus the following LDPE material parameters and IUPAC experimental data [12] were used in our calculations:

$\varrho = 918\ \mathrm{kg/m^2}$, $C = 2.302 \cdot 10^3\ \mathrm{m^2/s^2\,K}$,
$\varkappa = 0.26\ \mathrm{kg\,m/s^3\,K}$, $\eta_0 = 5.5 \cdot 10^4\ \mathrm{kg/ms}$,
$R = 1.5\ \mathrm{mm}$, $E_0 = 57.7\ \mathrm{kJ/mole}$, $T_0 = T_w = 150\,°\mathrm{C}$,

and the parameters a_k, λ_k and β_k are the same as for constant temperature $T_0 = 150\,°\mathrm{C}$, see [7] and [10]. The extrusion experiment was basically an isothermal one and it is difficult, if not impossible, to find out and impose the exact experimental thermal boundary conditions in numerical modelling. To start with, the thermal boundary conditions shown in figure 1 were con-

sidered to be reasonable. Note from figure 1 that the inlet temperature is assumed uniform and here we anticipate a thermal developing flow in the inlet region. As we will see later the fully developed temperature profile was never reached because of the very limited inlet length and the cooling effect down stream on the free surface.

3.2 Results and discussion

We first did the calculation for $\bar{D} = 1.0\ s^{-1}$ where our isothermal simulation [10] predicted the swelling ratio to be $\chi = 1.51$ compared with experimental value of 1.52. This good agreement indicates that unless the thermal boundary conditions used were very close to experimental conditions which were basically isothermal, non-isothermal simulation at $\bar{D} = 1.0\ s^{-1}$ would be worse than the isothermal one. For convenience, we used $\bar{W} = R\,\dot{\gamma}_w/4$ as the characteristic velocity of the flow, where $\dot{\gamma}_w$ is the shear rate on the die wall upstream [7]. In the Newtonian case, $\bar{W}$ is simply the average velocity. While the proper value of the Nusselt number $R\,h/\varkappa$ still remains a question, in the first instance we adopt the value $Nu = 0.72$, as used in other works [2, 4]. This value was obtained by Acierno *et al.* [17] from melt spinning measurements for polyethylene. As we will see later from the resulting cooling effect this value is too large for the present extrusion problem, which is clearly due to the fact that the motion involved in the extrusion experiments is much slower than that in the melt spinning process and the same heat transfer coefficient will cause excessive cooling to the extrudate. We found, however, that a much more appropriate value $Nu = 0.023$ could be calculated from the heat transfer coefficient h_c obtained from our own film blowing calculation [5], where an inverse method was used to find h_c by matching the experimental temperature at the freezing line [5, 18]. When using the value 0.72 for Nu, the non-isothermal calculation for $\bar{D} = 1.0\ s^{-1}$ gave $\chi = 1.42$, not as good as the isothermal prediction. The reason for the failure of non-isothermal simulation at $\bar{D} = 1.0\ s^{-1}$ can easily be found out by checking the solution for the temperature field: the minimum temperature on the free surface was down to about 55 °C which was 95 °C less than the wall temperature and well below the LDPE melting temperature. This is certainly far away from actual experimental reality and simply means the value 0.72 for the Nusselt number was too large and therefore the cooling was unrealistically strong. Note in a similar non-isothermal calculation for the Newtonian case [2, 4] with the same Nusselt number value, the maximum temperature decrease was about the 65 °C at an

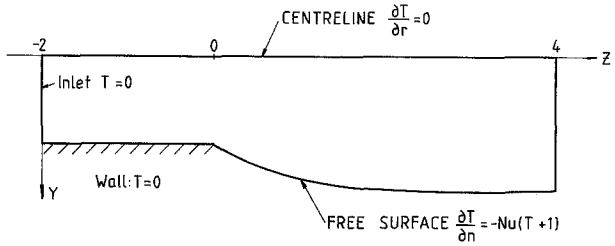

Fig. 1. Geometry and thermal boundary conditions for extrusion calculation (T is dimensionless)

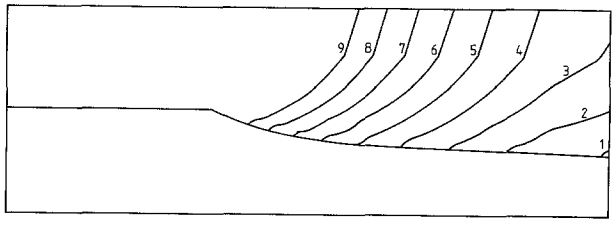

Fig. 2. Dimensionless temperature contours for $\bar{D} = 1\ s^{-1}$ case with $Nu = 0.72$. Contour values are given by $T^* = -0.76 + 0.06\,(I-1)$, where I is the contour number

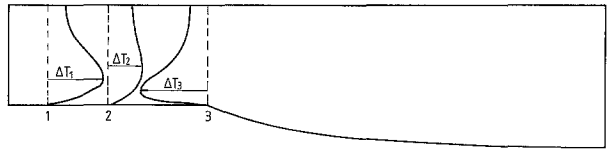

Fig. 3. Temperature profiles for $\bar{D} = 1\ s^{-1}$ case with $Nu = 0.72$. A much larger scale is used for profile No. 3: $\Delta T_1 = 2.7 \cdot 10^{-3}$ C, $\Delta T_2 = 1.5 \cdot 10^{-3}$ C, $\Delta T_3 = -4$ °C

average velocity $\bar{V} = 1$ mm/s, and also the smaller the average velocity was, the larger the temperature decrease was as could be expected. In the present case at $\bar{D} = 1.0\ s^{-1}$ the average velocity was $\bar{V} = R\bar{D}/4 = 0.375$ mm/s. Also note in the Newtonian case the same LDPE data were used and the Péclet number defined in terms of average velocity was 6.324 when $\bar{V} = 1$ mm/s while in the present case at $\bar{D} = 1.0\ s^{-1}$ the Péclet number is 4.568. So with the same dimensionless heat transfer coefficient the temperature decrease in the two cases are qualitatively compatible. Figure 2 shows the dimensionless temperature contours for $\bar{D} = 1.0\ s^{-1}$, this contour is very similar to that obtained in the Newtonian case at $\bar{V} = 1$ mm/s. Note in figure 2 the free surface far down-stream is not completely parallel to the centreline, which is probably due to the fact that before the free surface becomes 'flat', the melt under excessive cooling gets too stiff to deform.

Although the non-isothermal calculation at $\bar{D} = 1.0\ s^{-1}$ with $Nu = 0.72$ was not realistic because the temperature solution was well out of the possible practical range, it very well illustrated the hot layer effect. Figure 3 plots temperature profiles at three sections

within the die tube, among them No. 3 is right at the exit plane. Initially the temperature is uniform throughout, for very short times there is no heat conduction and the temperature rises directly in proportion to the dissipation rate of mechanical energy. As shown by profile No. 1 in figure 2 the maximum temperature rise is near the wall since the shear rate is highest there. Further downstream profile No. 2 shows that the heat conductivity of the melt has acted to smooth out the temperature profile, causing the maximum point to move towards the centreline. If the tube length is long enough the conduction will in the end balance generation and the temperature will be highest at the centre when fully developed. But such is not the case in the present problem: before the temperature is fully developed the thermal boundary condition as well as the kinematic boundary condition changes and the heat loss at the free surface affects the temperature profiles near the die exit inside the die tube through conduction. Here we have a very strong heat loss at the free surface and a very weak self-heating since the Brinkman number in this case is in the order of 10^{-4}. The consequence is that the heat loss on the free surface becomes the dominating factor in determining the temperature profile near the die exit and thus the self-heating is unimportant to die swell in this problem. In fact we did the same calculation without self-heating and the swelling ratio was virtually the same. Profile No. 3 shows the temperature distribution at the exit plane. We see the pattern of this profile is totally different from that of the two in the upstream region. As a result of heat loss the temperature at exit plane is everywhere lower than wall temperature and an effective "hot layer" is formed near the die wall. It is this hot layer, according to the inelastic swelling mechanism, that caused the swelling ratio to decrease from 51% to 42%. Note that the scale for plotting profile No. 3 is more than two orders larger than that for the other two profiles, which means even if one linearly superimposes the fully developed temperature profile due to self-heating onto profile No. 3, it will have no noticeable change at all, schematically showing the unimportance of self-heating in this particular case.

For a more realistic non-isothermal modelling, we next used the heat transfer coefficient h_c obtained from our own film blowing calculation for calculating the Nusselt number. This time with $Nu = 0.023$ the predicted swelling for $\bar{D} = 1.0\ s^{-1}$ was up to 50%, very close to isothermal prediction and the experimental value. The maximum temperature decrease on the free surface was about 8 °C, much more realistic than the previous calculation with $Nu = 0.72$. The 'flat' free surface condition far down-stream is now satisfied by the solution and the temperature contour and the development of temperature profiles were qualitatively very similar to those shown in figures 2 and 3, due to using the same Péclet number, Brinkman number and Nahme-Griffith number, as shown in figures 4 and 5. However, the cooling effect on the temperature distribution at the die exit as well as inside the die tube was so much weaker than in the previous case that no effective hot layer was formed: at the die exit plane the maximum temperature difference was only about 0.2 °C, thus the rheological process up to die exit could be considered as a basically isothermal one, as the predicted swelling ratio suggested. We note again in figure 5 a different scale is used for plotting profile No. 3. To see the separate effect of self-heating we also did a calculation for the same $\bar{D} = 1.0\ s^{-1}$ case but with a zero heat transfer coefficient, i.e., with an insulated free surface. This is an extreme case but is believed to be closer to experimental reality than using the value $Nu = 0.72$ for heat transfer on the free surface. Results with zero Nu value showed that the temperature profile at the die exit plane was similar to those developing ones upstream and the calculated swelling ratio was back to the isothermal value. This is not unexpected since the temperature variation due to self-heating is small and the whole rheological process inside and outside the die tube is essentially isothermal.

At high apparent shear rate $\bar{D} = 10\ s^{-1}$, the Péclet number in terms of average velocity is 10 times as large as at $\bar{D} = 1.0\ s^{-1}$, where the average velocity is given by $\bar{V} = R\bar{D}/4$ from the definitions of $\bar{V}$ and $\bar{D}$. This larger

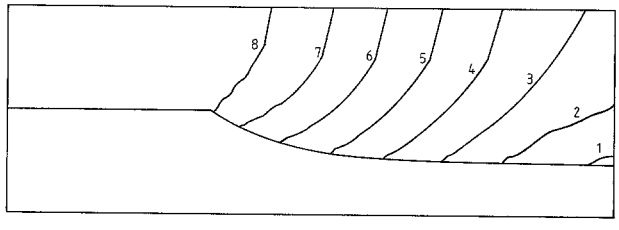

Fig. 4. Dimensionless temperature contours for $\bar{D} = 1\ s^{-1}$ case with $Nu = 0.023$. Contour values are given by $T^* = -0.06 + 0.08\,(I-1)$, where I is the contour number

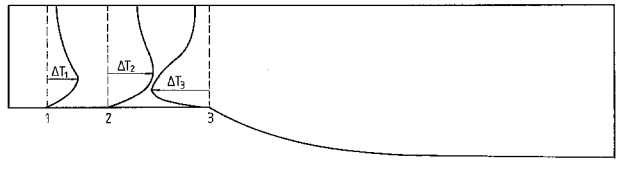

Fig. 5. Temperature profiles for $\bar{D} = 1\ s^{-1}$ case with $Nu = 0.023$. A larger scale is used for profile No. 3: $\Delta T_1 = 2.8 \cdot 10^{-3}$ C, $\Delta T_2 = 4.0 \cdot 10^{-3}$ C, $\Delta T_3 = -0.18$ °C

Péclet number will bring some new features to the solution since we know in general terms that the effect of the heat transfer boundary condition is greatly affected by the Péclet number. The Nahme-Griffith number at $\bar{D} = 10\ s^{-1}$ is about 0.19. For comparation, we did the non-isothermal calculation for $\bar{D} = 10\ s^{-1}$ with the Nusselt number $Nu = 0.023$, i.e., the one calculated from the film blowing heat transfer coefficient, as for the $\bar{D} = 1\ s^{-1}$ case. With this value the calculated swelling ratio showed a negligible difference from the isothermal prediction (Table 1). This result at first seemed to be a little surprising to us since in this case we expected a much stronger coupling between momentum and energy equations and an effective outer hot layer to bring the swelling ratio down. However, with a little study of the temperature field for $\bar{D} = 10\ s^{-1}$, a satisfactory explanation can be found by noting the following two new features in the solution: firstly the temperature distribution at the die exit is not affected any more by the cooling on the free surface; secondly with the same Nusselt number as at $\bar{D} = 1\ s^{-1}$ the cooling itself at $\bar{D} = 10\ s^{-1}$ is much weaker due to a larger Péclet number. In figure 6 is shown the dimensionless temperature contours for the $\bar{D} = 10\ s^{-1}$ case. Compared with figures 2 or 4, immediately we note the pattern of the contours in figure 6 is very different. The contours for $\bar{D} = 10\ s^{-1}$ show that the axial temperature gradient is very small, much smaller than the $\bar{D} = 1.0\ s^{-1}$ case, clearly indicating that the axial convection dominates and the axial conduction is relatively very weak, as it can be expected from the larger Péclet number. Under this axial convection domination, heat transfer on the free surface will have very little effect on the temperature distributions at the die exit and upstream inside the die tube. The heat loss on the free surface only causes a large temperature gradient in the radial direction near the free surface. Figure 7 plots the temperature profiles for $\bar{D} = 10\ s^{-1}$ case at three sections, one at the exit plane and two inside the die tube. Note this time one single scale is used for all three profiles. Compared with figures 3 or 5 for the $\bar{D} = 1\ s^{-1}$ case, the developing temperature profiles in figure 7 are sharper because of a higher temperature concentration near the wall due to a larger Brinkman number and a slower temperature development due to the larger Péclet number. A qualitative difference between the two cases is seen near the die exit. In the $\bar{D} = 1.0\ s^{-1}$ case (figures 3 and 5) where the Péclet number is not so large the cooling on the free surface greatly affects temperature distributions near the die exit through conduction. Despite the weak self-heating the average temperature begins to decrease near the die exit until the temperature becomes much lower than the wall temperature everywhere and a hot layer forms at the die exit due to the constant wall temperature. In the $\bar{D} = 10\ s^{-1}$ case (figure 7) the Péclet number is 10 times as large, the temperature developing process is little affected by the cooling on the free surface due to convection domination: the maximum temperature point moves very slowly towards the centreline and the average temperature across a section increases all the way down to the exit plane. At the exit plane, the temperature is still basically a developing one similar to those upstream, showing little cooling effect from the free surface, the temperature variation due to self-heating alone is still very small ($Br = 0.04$) and no effective hot layer is formed in the outer layer. Thus it is not surprising that the non-isothermal calculation predicted a swelling ratio not much different from the isothermal value if we also note that the maximum temperature decrease on the free surface as the result of cooling in this case is only about 2 °C. Finally, we did a calculation with a zero Nusselt number for the

Table 1. Results for LDPE swelling with various thermal boundary conditions for two values of $8\ \bar{V}/D$: 1.0 and $10\ s^{-1}$. The second column gives experimental results

$\bar{D}\ (s^{-1})$	IUPAC data	isothermal prediction	non-isothermal prediction		
			$N_u = 0.72$	$N_u = 0.023$	$N_u = 0.0$
1.0	1.52	1.51	1.42	1.50	1.51
10	1.56	1.84	–	1.85	1.84

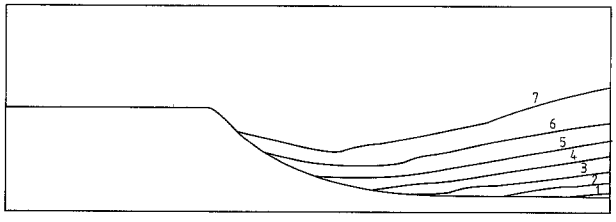

Fig. 6. Dimensionless temperature contours for $\bar{D} = 10\ s^{-1}$ case with $Nu = 0.023$. Contour values are given by $T^* = -0.014 + 0.002\ (I - 1)$, where I is the contour number

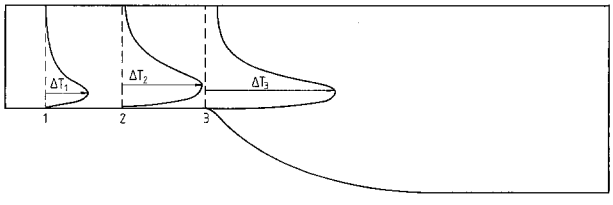

Fig. 7. Temperature profiles for $\bar{D} = 10\ s^{-1}$ case. Same scale is used for all three profiles: $\Delta T_1 = 3.5 \cdot 10^{-3}$ C, $\Delta T_2 = 5.3 \cdot 10^{-2}$ C, $\Delta T_3 = 8.6 \cdot 10^{-2}$ C

$\bar{D} = 10\ s^{-1}$ case. As the temperature variation throughout is caused by self-heating alone which is very weak, again the isothermal swelling ratio value resulted. The calculated swelling ratio values for all the cases reported in this paper are given in table 1, along with the isothermal predictions and experimental data.

4. Concluding remarks

In this work the Morland-Lee hypothesis is applied to a specific form of the KBKZ model and a pseudo-time integral scheme based on the streamline element method [4, 7] has been developed to combine variable temperature with viscoelasticity. The simultaneous calculation of both the observer time and pseudo-time is essential to simplify the procedures of dealing with the mixed feature of the time-temperature shifting formulation. The conclusions that can be drawn from the non-isothermal modeling of extrusion experiment are as follows:

a) The temperature variation may not be considered as the main reason for the disagreement between isothermal calculation [7, 10] and experiment at high apparent shear rate $\bar{D} = 10\ s^{-1}$. Unless more exact thermal conditions are known the isothermal assumption is a good approximation throughout the experimental range.

b) The self-heating in these particular IUPAC extrusion experiments is not important. Although the apparent shear rate reached in the experiments is not small, the average velocity is always very small due to the small radius of the die tube used. This is why self-heating is insignificant even at significant shear rates, which is an important factor to be considered in achieving thermal similarity in model experiments of extrusion.

c) The heat transfer boundary condition on the free surface may or may not be important in controlling the temperature distribution near the die exit plane, depending on whether the Péclet number is small or large. Only when the Péclet number is not large can the cooling on the free surface have a dominant control on the temperature distribution near the die exit.

d) The hot layer effect was confirmed by our full non-isothermal and non-Newtonian finite element simulation. The formation of the effective outer hot layer is not necessarily through self-heating at the die wall.

The numerical simulation of non-isothermal and non-Newtonian flow is just at its beginning [1, 13] and much remains to be done to gain a better understanding of the interaction between variable temperature and viscoelasticity. As a final remark, we need to be cautious over the too-enthusiastic use of the time-temperature shifting idea [1, 14–16].

Acknowledgement

We acknowledge the Australian Research Grants Scheme for supporting this work and the University of Sydney for providing a postgraduate scholarship for one of the authors.

References

1. Tanner RI (1985) Engineering Rheology. Oxford University Press
2. Phuoc HB, Tanner RI (1980) J Fluid Mech 98:253
3. Tanner RI (1980) J Non-Newtonian Fluid Mech 6:289
4. Luo XL, Tanner RI (1986) J Non-Newtonian Fluid Mech 21:179
5. Luo XL, Tanner RI (1985) J Polym Engng Sci 25: 320
6. Morland LW, Lee EH (1960) Trans Soc Rheol 4:233
7. Luo XL, Tanner RI (1986) J Non-Newtonian Fluid Mech 22:61
8. Kearsley EA (1962) Trans Soc Rheol 6:253
9. Papanastasiou AC, Scriven LE, Macosko CW (1983) J Rheol 27:387
10. Luo XL, Tanner RI (1987) Int J Num Meth Engng, to appear
11. Huynh BP (1983) J Non-Newtonian Fluid Mech 13:1
12. Meissner J (1975) Pure and Applied Chemistry 42:551
13. Pearson JRA, Richardson SM (1983) Computational Analysis of Polymer Processing. Applied Science Publications, London
14. Collins EA, Metzger A (1970) Polym Engng Sci 10:57
15. Christensen RM (1971) Theory of Viscoelasticity. Academic Press, New York
16. Matsumoto T, Bogue DC (1977) Trans Soc Rheol 21:453
17. Acierno D, Dalton JN, Rodriguez JM, White JL (1971) J Appl Polym Sci 15:2395
18. Gupta RK (1981) Ph.D Thesis, University of Delaware

(Received March 13, 1987)

Authors' address:

X.-L. Luo, Prof. R. I. Tanner
Department of Mechanical Engineering
University of Sydney
Sydney, N.S.W. 2006 (Australia)